Visualization of Higher-Order Topological Insulating Phases in Two-Dimensional Dielectric Photonic Crystals

Bi-Ye Xie,[1,2,‡] Guang-Xu Su,[1,3,‡] Hong-Fei Wang,[1,2,‡] Hai Su,[1,3] Xiao-Peng Shen,[4] Peng Zhan,[1,3,5,*] Ming-Hui Lu,[1,2,6,5,†] Zhen-Lin Wang,[1,3,5] and Yan-Feng Chen[1,2,5]

[1]*National Laboratory of Solid State Microstructures, Nanjing University, Nanjing 210093, China*
[2]*Department of Materials Science and Engineering, Nanjing University, Nanjing 210093, China*
[3]*School of Physics, Nanjing University, Nanjing 210093, China*
[4]*School of Physical Science and Technology, China University of Mining and Technology, Xuzhou 221116, China*
[5]*Collaborative Innovation Center of Advanced Microstructures, Nanjing University, Nanjing 210093, China*
[6]*Jiangsu Key Laboratory of Artificial Functional Materials, Nanjing 210093, China*

(Received 20 December 2018; revised manuscript received 19 March 2019; published 14 June 2019)

The studies of topological phases of matter have been developed from condensed matter physics to photonic systems, resulting in fascinating designs of robust photonic devices. Recently, higher-order topological insulators have been investigated as a novel topological phase of matter beyond the conventional bulk-boundary correspondence. Previous studies of higher-order topological insulators have been mainly focused on the topological multipole systems with negative coupling between lattice sites. Here we experimentally demonstrate that second-order topological insulating phases without negative coupling can be realized in two-dimensional dielectric photonic crystals. We visualize both one-dimensional topological edge states and zero-dimensional topological corner states by using the near-field scanning technique. Our findings open new research frontiers for photonic topological phases and provide a new mechanism for light manipulating in a hierarchical way.

DOI: 10.1103/PhysRevLett.122.233903

Introduction.—One of the most intriguing developments of condensed matter physics over the past few decades has been the discovery of topological phases in electronic systems [1,2], which has been recently developed in photonics [3–14] and phononics [15–20]. A key feature of the topological insulators is the backscattering-immune edge states, which are robust against perturbations and provide potential designs of various topological devices [3–6,17,19]. According to the bulk-boundary correspondence, n-dimensional (nD) topological insulators (TIs) have $(n-1)$D edge states [21]. However, a new kind of TIs defined as higher-order topological insulators (HOTIs) have been recently proposed in tight-binding models in electronic systems which go beyond the traditional bulk-boundary correspondence [22–36]. The mth-order TIs have nD gapped bulk states and $(n-1)$D, $(n-2)$D, …, $(n-m-1)$D gapped edge states while having $(n-m)$D gapless edge states. The arising of these lower-dimensional topological edge states can either stem from the quantization of quadrupole moments such as the topological quadrupole insulators [22], which have been realized in mechanics [23], microwave systems [24], and topolectrical circuits [25], or stem from the quantization of the dipole moments [22] such as the HOTIs in a 2D breathing kagome lattice [29], which have been realized in sonic crystals [33–35] and a waveguide array [32].

Photonic crystals (PCs) offer irreplaceable opportunities to investigate theoretical physics in a highly controllable way [37,38]. Moreover, they have a wide range of applications in manipulating the propagation of electromagnetic (EM) waves and designing novel photonic devices from microwaves to optical waves. Previously, topological insulating phases in dielectric PCs have been experimentally demonstrated with traditional bulk-boundary correspondence (the first-order TIs) [39]. A recent theoretical study shows that it is possible to realize HOTIs in 2D pure-dielectric PCs [30]. However, the experimental realizations of HOTIs in pure-dielectric PCs without negative coupling are still challenging and waiting to be achieved.

In this Letter, we experimentally realize a second-order topological insulator (SOTI) in a 2D dielectric PC which is based on the 2D extension of the Su-Schrieffer-Heeger (SSH) lattice [40–43]. Instead of introducing a negative coupling, which is essential to the formation of topological quadrupole insulators, we demonstrate that the quantization of dipole moments in the C_4 symmetric lattice can also lead to second-order topological insulating phases. We engineer a square metastructure formed by two pieces of PCs, where the inner PC is in a topological nontrivial phase while the outer PC is in a topological trivial phase. By applying the near-field scanning technique, we visualize both the first-order and the second-order topological insulating phases in the same structure, which can be simply controlled by the geometric parameters, implying a hierarchical structure in topological insulating phases [36].

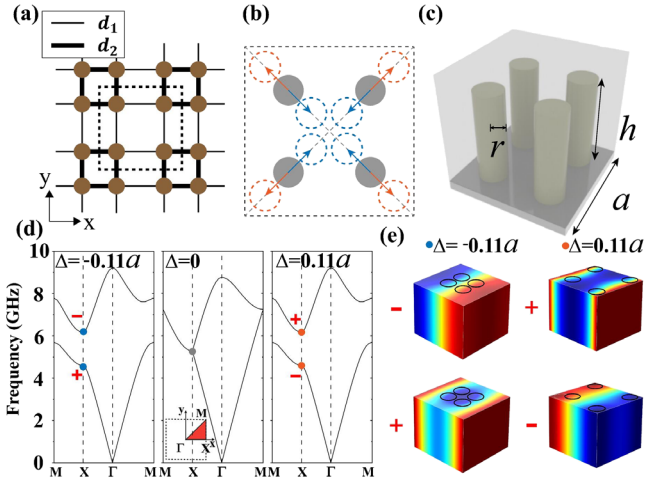

FIG. 1. Crystal structures and bulk band structures. (a) The lattice structure with d_1 and d_2 representing the intracell distance and intercell distance, respectively, of the nearest atoms. (b) Different configurations of photonic crystals. The dashed blue (red) circles represent the shrunken (expanded) configuration, and gray circles represent the normal square lattice without tetramerization. (c) Three-dimensional structure of a unit cell with the upper plate removed. (d) Band structures for $\Delta = -0.11a$ (left), $\Delta = 0$ (middle), and $\Delta = 0.11a$ (right), which represent a shrunken, normal, and expanded lattice, respectively. For shrunken and expanded lattices, the band structures have the same dispersion but different parities of the first and second bands at the X point (denoted by $+$ and $-$ symbols). (e) The electric field distributions in a unit cell of the first band (lower panels) and the second band (upper panels) at the X points in the first Brillouin zone which show the parities.

Crystal structure and bulk band structure.—Our 2D PCs possess a square lattice geometry with four artificial atoms formed in a unit cell as depicted in Fig. 1(a). There are two competing parameters in a PC: the intracell distance of nearest atoms d_1 and the intercell distance of nearest atoms d_2. d_1 and d_2 modulate the coupling strengths between nearest lattice sites, and we notice that $d_1 + d_2 = a$, where a is the lattice constant. For simplicity, we define $\Delta = (d_1 - d_2)/4$, which determines the lattice structure of a PC if other parameters are fixed. In this Letter, we consider PCs with a finite height in the z direction and set the height of cylinders $h = 13.5$ mm, lattice constant $a = 20$ mm, and radius of the cylinders $r = 2.4$ mm as shown in Fig. 1(c).

Next, we show the evolution of band gaps for transverse magnetic modes by numerical simulation. In this Letter, we consider perfect electric conductor (PEC) boundaries in the upper and lower plates perpendicular to the z direction [see Fig. 1(c)] and set the relative dielectric permittivity $\epsilon = 6.1$. The above implementations ensure a valid 2D approximation. We start from a simple case where $\Delta = 0$ [indicated by gray circles in Fig. 1(b)], and the PC is a conventional 2D square lattice PC (with one atom in the unit cell). In this case, the first band and the second band are degenerate at the X point as shown in Fig. 1(d) (middle panel). Next, we consider two cases: $\Delta = -0.11a$, which corresponds to the "shrunken" lattice [indicated by dashed blue circles in Fig. 1(b)], and $\Delta = 0.11a$, which corresponds to the "expanded" lattice [indicated by dashed red circles in Fig. 1(b)]. In both cases, the previous gapless point is opened and a full photonic band gap emerges. The band structures for these three cases are presented in Fig. 1(d). We notice that the shrunken lattice and expanded lattice are in distinct topological phases which are connected by a band-inversion process. To demonstrate it clearly, we calculate the electric field distribution of the unit cell for two cases as shown in Fig. 1(e). Because of the inversion symmetry, the parities of the first band and the second band can be defined as the eigenvalues of the inversion operator. As shown in Figs. 1(d) and 1(e), the parities for the first and the second bands have changed as we change $\Delta = -0.11a$ to $\Delta = 0.11a$, indicating the bands have been inverse.

Topological phase transition induced by deformation of the lattice structure.—Here we investigate the relation between the size of the gap and Δ. The result (phase diagram) is given in Fig. 2(a). It is intriguing to notice that there is a metallic phase other than two insulating phases for $\Delta \neq 0$. Although the local gapless point at X is opened, the gap in the first Brillouin zone does not appear when $|\Delta|$ is relatively small. The phase diagram is similar to the theoretical tight-binding model (2D SSH model) [30,42], indicating a topological equivalence between the band structures of our PCs and those of the 2D SSH model (see Sec. I in Ref. [44]). From the perspective of the tight-binding approximation, when Δ is nonzero, a tetramerized configuration of the nearest-neighbor coupling is formed,

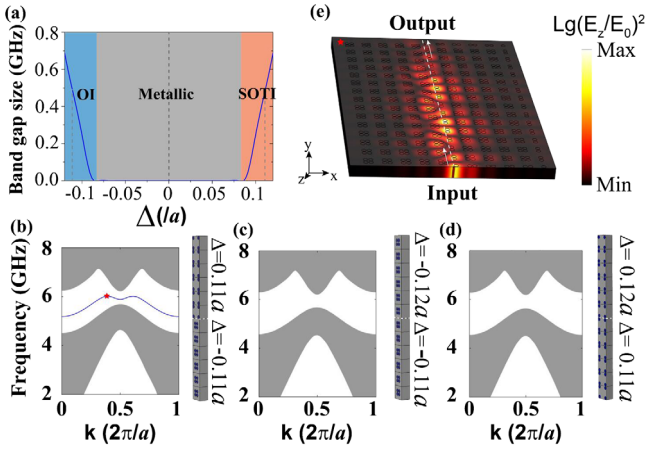

FIG. 2. Phase diagram and topological edge states. (a) The OI phase, metallic phase, and SOTI phase with different Δ. (b) The projected band structure of two photonic crystals within different topological phases. A band gap with a 1D edge state is presented. (c),(d) The projected band structure of two photonic crystals within the same trivial and nontrivial phases, respectively. There is no edge state in the gap. (e) A simulated edge state with a frequency at 6.00 GHz [represented by a red star in (b)].

and the mass term in the effective Hamiltonian describing the low-energy physics around the gapless point is nonzero. We found two areas of fully gapped phases when $\Delta < -0.087a$ and $\Delta > 0.087a$, which are represented by blue and red, respectively, in Fig. 2(a). These two areas have two mass terms with different signs, respectively, and, hence, are topological distinct to each other. Since the gap is maintained in each individual area, the band structures can be connected by adiabatic evolutions and, thus, belong to the same topological class.

To characterize the topological properties of the 1D edge states, we define a topological invariant based on the 2D polarization. The topological phases can be characterized by

$$P_i = -\frac{1}{(2\pi)^2}\int_{BZ} d^2\boldsymbol{k}\mathrm{Tr}[\hat{\mathcal{A}}_i], \qquad i = x, y, \qquad (1)$$

where $(\hat{\mathcal{A}}_i)_{mn}(\mathbf{k}) = i\langle u_m(\mathbf{k})|\partial_{k_i}|u_n(\mathbf{k})\rangle$, with m and n running over all bands below the gap. $|u_m(\mathbf{k})\rangle$ is the periodic part of the electric field for the mth band. The 2D polarization is simply related to the 2D Zak phase via $\theta_i = 2\pi P_i$ for $i = x, y$. For $\Delta > 0.087a$, $\boldsymbol{P} = (P_x, P_y) = (\frac{1}{2}, \frac{1}{2})$, which implies that the PC is in a topological nontrivial insulating phase. Similarly, when $\Delta < -0.087a$, $\boldsymbol{P} = (P_x, P_y) = (0, 0)$, which implies that the PC is in a topological trivial phase. The above polarization forms a $\mathbb{Z}_2$ topological invariant of the system (see Sec. II in Ref. [44]).

To demonstrate the existence of edge states, we consider a combined structure of PCs where a topologically nontrivial PC is jointed by a topologically trivial PC. The simulated projected band structure is shown in Fig. 2(b). We use the PEC boundary condition for boundaries parallel to the interface of two PCs, which ensures that there is no extra edge state (see Sec. V in Ref. [44]), while using Floquet periodic boundary condition for boundaries perpendicular to the interface and set other parameters the same as those in Fig. 1. As seen in Fig. 2(b), an interface state (indicated by the solid blue line) appears in the middle of the gap. For comparison, we provide the projected band structures of two PCs in the same topological phases as shown in Figs. 2(c) and 2(d) which have no edge states. The simulated field distribution of the combined structure for the nontrivial case is shown in Fig. 2(e). A 1D localized state emerges and decays fast away from the interface (indicated by the white dashed line).

Experimental observation of corner states in a metastructure.—We now extend the discussion from the previous combined structure to a square metastructure as shown in Fig. 3(a). The metastructure is realized by placing a topological nontrivial PC (denoted as SOTI) with 10×10 periods, surrounding by a four-layer trivial PC [denoted as an ordinary insulator (OI)]. Δ for the SOTI and OI are $0.11a$ and $-0.11a$, respectively, with other geometric parameters the same as those in Fig. 1. The SOTI and

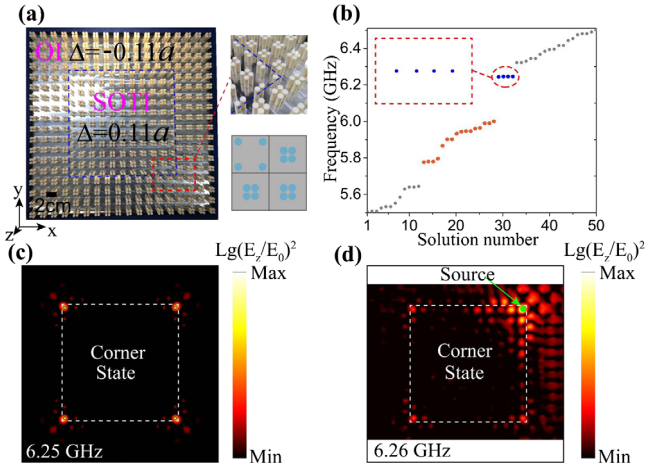

FIG. 3. Experimental visualization of corner states in a metastructure. (a) Photograph of a metastructure with the upper metallic plate removed. The boundary of two photonic crystals is denoted by the blue dashed line. The enlarged corner structure is presented. (b) Eigenmodes calculation of the metastructure with the same parameters in Fig. 1(d). Corner states, edge states, and bulk states are represented by blue, yellow, and gray dots, respectively. (c) A simulated electric field distribution of one of the four corner states. (d) Experimental visualization of corner states at 6.26 GHz. The scanning area is a rectangle instead of a square. The excitation source is depicted by the green dot.

OI are distinct in topology, and their band gaps overlap with each other. Figure 3(b) shows the eigenmodes of the metastructure at frequencies between 5.50 and 6.50 GHz. The numerical calculation with the PEC boundary condition for boundaries in the x and y directions indicates that four near-degenerate midgap states (indicated by blue dots) emerge at frequencies around 6.25 GHz between the 1D edge states (indicated by yellow dots) and the bulk bands (indicated by gray dots). The simulated electric field (polarized in the z direction) distribution is shown in Fig. 3(c), which clearly demonstrates that these four states are strongly localized at four corners of the box-shape boundary (indicated by the white dashed line) in the metastructure. The phases of the corner states form both a dipole and a quadrupole (see Sec. IV in Ref. [44]).

To experimentally observe corner states, we fabricate a metastructure of PCs consisting of alumina cylinders with relative dielectric permittivity $\epsilon = 10$. To prevent the transverse magnetic modes from leaking into the air, we use two flat metallic plates to cover the bottom and top of the PCs, mimicking the PEC boundaries. We then place an excitation source at the upper-right corner of the boundary of two PCs as depicted in Fig. 3(d). By using near-field scanning technology, we obtain quantitatively the distribution of the out-of-plane electric field (polarized in the z direction) along the whole interface and visualize the result obtained at 6.26 GHz as depicted in Fig. 3(d). See details in Sec. VII in Ref. [44].

Figure 3(d) shows a strong concentration of field distribution in four dielectric cylinders at the corners of

metastructure, indicating the subwavelength character of the corner states. An enhancement of fields from the source is observed. The corner states arise due to the filling anomaly in C_4-symmetric topological crystalline insulators [45]. Based on the C_4 symmetry representations at a high symmetry point, we can define a corner topological index:

$$Q^c = \frac{1}{4}([X_1] + 2[M_1] + 3[M_2]), \tag{2}$$

where $[\Pi_p] = \#\Pi_p - \#\Gamma_p$ and $\#\Pi_p$ is defined as the number of bands below the band gap with rotation eigenvalues $\Pi_p = e^{[2\pi i(p-1)]/4}$ for $p = 1, 2, 3, 4$. Π stand for high symmetric points X, M, and Γ. For the nontrivial case, we have $[X_1] = -1$, $[M_1] = 1$, and $[M_2] = 0$. Therefore, the corner topological index is $Q^c = \frac{1}{4}$, indicating $\frac{1}{4}$ fractionalized corner states at each of the four corners (see Sec. II in Ref. [44]). A small difference of frequencies between simulations and experiments is induced by an air layer above the PCs (see Sec. VI in Ref. [44]) and manufacturing accuracy errors.

Hierarchical topological insulating phases in photonics.—To further verify the coexistence of 1D topological edge states and 0D topological corner states, we excite the eigenstates from 5.23 to 6.70 GHz. The same procedure is applied as the previous section to observe the out-of-plane electric field distribution. The result is shown in Fig. 4. The local field intensity for bulk, edge, and corner points (represented by a gray, yellow, and blue dot in the inset, respectively) are obtained from the averaged value of field distributions at each point, respectively, as depicted in Fig. 4(a). We note that a nonzero intensity at a corner (edge) point can stem from the existence of edge states (bulk states). We find that there is a bulk-edge-corner-bulk evolution as we continuously increase the excitation frequencies. This measurement agrees with the result shown in Fig. 3(b). A small difference in the frequencies between the simulation and experiment is observed due to the air layer above the metastructure in experiments. As shown in Fig. 4(c), the field strength in the 2D bulk of the metastructure is significantly suppressed, representing the gapped 2D bulk states. Meanwhile, a strong field strength at the 1D boundaries is obviously observed, which demonstrates the gapless 1D edge states. These features match with the traditional bulk-boundary correspondence and the definition of the first-order topological insulators. Similarly, in Fig. 4(d), the field strength at the 0D corners is strong, and the field strength in the 1D boundaries as well as 2D bulk of the structure (except from the source) are significantly weak, which clearly demonstrates a SOTI phase as its definition. Because of the linear dispersion of the first band near the Γ point in dielectric PCs, the chiral symmetry is broken, and the band structure is beyond the scope of the tight-binding model with nearest-neighbor couplings. Therefore, the frequency levels of the edge states and corner states are deviated from the "zero energy" level

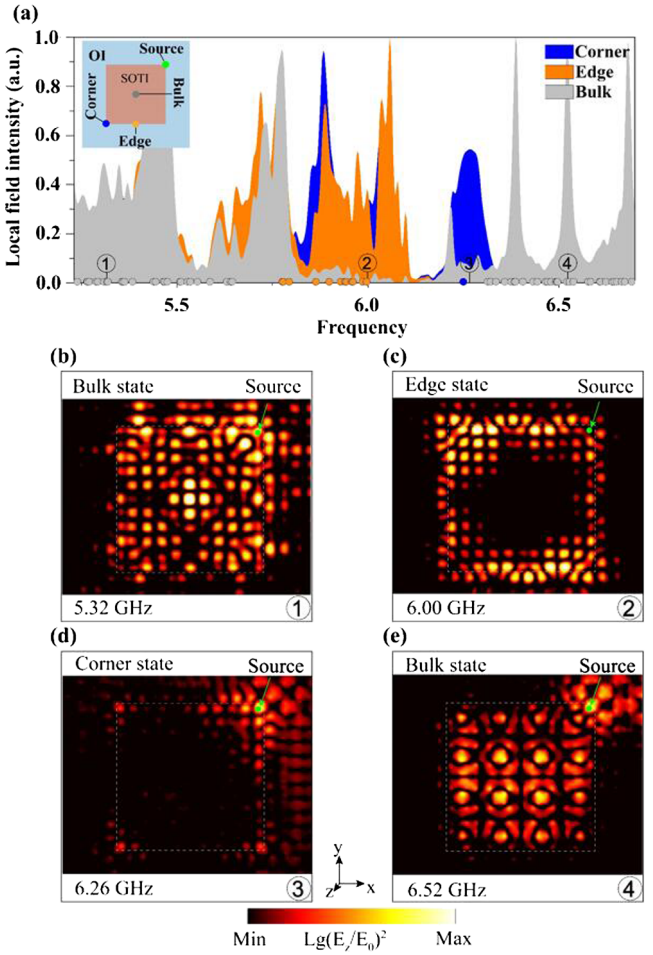

FIG. 4. Hierarchical structure of topological insulating phases. (a) Normalized local field intensity measured at bulk, edge, and corner points as depicted in the inset. The bulk, edge, and corner eigenstates from the numerical calculation are represented by gray, yellow, and blue dots, respectively. We provide the visualization of (b) a bulk state at 5.32 GHz, (c) an edge state at 6.00 GHz, (d) a corner state at 6.26 GHz, and (e) a bulk state at 6.52 GHz with the excitation source placed at the upper-right corner of the boundary (represented by the white dashed line).

and can be separated from the bulk bands (that appear in the band gap). These topological states are robust against disorders which do not break the C_4 symmetry.

Conclusion and discussion.—In summary, we here experimentally demonstrate a 2D SOTI in dielectric PCs and visualize both 1D topological edge states and 0D subwavelength corner states. Our realization is based on pure-dielectric PCs, which have no undesirable Ohmic-loss effect compared to those with metallic and plasmonic materials and play an important role in realizing photonic integrated circuits and resonator antennas with high radiation efficiency [39,52]. The hierarchical structure of topological insulating phases is observed in a topological nontrivial configuration [53]. These structure-controlled topological phases may pave the way for the realization of 3D photonic HOTIs and higher-order topological

semimetals [54]. Moreover, the coexistence of different dimensional topological boundary states can serve as a basis for designing topological switch circuits between crystalline insulators and higher-order topological insulators [55]. Our implementation can be minimized, and the working frequency can be improved up to optical frequency by using microfabrication [56]. Finally, our findings may support explorations in designing a topological point source with lasering by introducing gain and loss in materials [57,58], topological light trappings [59], and photonic chips with multiphoton quantum states [60–62].

This work was financially supported by National Key R&D Program of China (Grants No. 2017YFA0303702 and No. 2018YFA0306202) and National Natural Science Foundation of China (Grants No. 11625418, No. 51732006, No. 11674166, and No. 11774162). B. X. thanks Xueyi Zhu for the useful discussions on the simulations.

Note added.—Independent of this work, other photonic realisations of corner states were simultaneously reported in two-dimensional photonic slabs [63], nanocavity [64], coupled waveguides [65], and with quadrupole phases [66].

*zhanpeng@nju.edu.cn
†luminghui@nju.edu.cn
‡B.-Y. X., G.-X. S., and H.-F. W. contributed equally to this work.

[1] M. Z. Hasan and C. L. Kane, Rev. Mod. Phys. **82**, 3045 (2010).
[2] X.-L. Qi and S.-C. Zhang, Rev. Mod. Phys. **83**, 1057 (2011).
[3] F. D. M. Haldane and S. Raghu, Phys. Rev. Lett. **100**, 013904 (2008).
[4] Z. Wang, Y. Chong, J. D. Joannopoulos, and M. Soljacic, Nature (London) **461**, 772 (2009).
[5] M. Hafezi, E. A. Demler, M. D. Lukin, and J. M. Taylor, Nat. Phys. **7**, 907 (2011).
[6] Y. Poo, R. X. Wu, Z. Lin, Y. Yang, and C. T. Chan, Phys. Rev. Lett. **106**, 093903 (2011).
[7] M. Hafezi, S. Mittal, J. Fan, A. Migdall, and J. M. Taylor, Nat. Photonics **7**, 1001 (2013).
[8] M. C. Rechtsman, J. M. Zeuner, Y. Plotnik, Y. Lumer, D. Podolsky, F. Dreisow, S. Nolte, M. Segev, and A. Szameit, Nature (London) **496**, 196 (2013).
[9] A. B. Khanikaev, S. H. Mousavi, W. K. Tse, M. Kargarian, A. H. MacDonald, and G. Shvets, Nat. Mater. **12**, 233 (2013).
[10] L. Lu, J. D. Joannopoulos, and M. Soljacic, Nat. Photonics **8**, 821 (2014).
[11] W. J. Chen, S. J. Jiang, X. D. Chen, B. Zhu, L. Zhou, J. W. Dong, and C. T. Chan, Nat. Commun. **5**, 5782 (2014).
[12] B. Y. Xie, H. F. Wang, X. Y. Zhu, M. H. Lu, Z. D. Wang, and Y. F. Chen, Opt. Express **26**, 24531 (2018).
[13] L.-H. Wu and X. Hu, Phys. Rev. Lett. **114**, 223901 (2015).
[14] L. Xu, H.-X. Wang, Y.-D. Xu, H.-Y. Chen, and J.-H. Jiang, Opt. Express **24**, 18059 (2016).
[15] Z. G. Chen, X. Ni, Y. Wu, C. He, X. C. Sun, L. Y. Zheng, M. H. Lu, and Y. F. Chen, Sci. Rep. **4**, 4613 (2014).
[16] Z. J. Yang, F. Gao, X. H. Shi, X. Lin, Z. Gao, Y. D. Chong, and B. L. Zhang, Phys. Rev. Lett. **114**, 114301 (2015).
[17] X. Ni, C. He, X. C. Sun, X. P. Liu, M. H. Lu, L. Feng, and Y. F. Chen, New J. Phys. **17**, 053016 (2015).
[18] M. Xiao, G. Ma, Z. Yang, P. Sheng, Z. Q. Zhang, and C. T. Chan, Nat. Phys. **11**, 240 (2015).
[19] C. He, X. Ni, H. Ge, X. C. Sun, Y.-B. Chen, M.-H. Lu, X.-P. Liu, and Y.-F. Chen, Nat. Phys. **12**, 1124 (2016).
[20] A. B. Khanikaev, R. Fleury, S. H. Mousavi, and A. Alu, Nat. Commun. **6**, 8260 (2015).
[21] T. L. Hughes, R. G. Leigh, and O. Parrikar, Phys. Rev. D **88**, 025040 (2013).
[22] W. A. Benalcazar, B. A. Bernevig, and T. L. Hughes, Science **357**, 61 (2017).
[23] M. Serra-Garcia, V. Peri, R. Süsstrunk, O. R. Bilal, T. Larsen, L. G. Villanueva, and S. D. Huber, Nature (London) **555**, 342 (2018).
[24] C. W. Peterson, W. A. Benalcazar, T. L. Hughes, and G. A. Bahl, Nature (London) **555**, 346 (2018).
[25] S. Imhof, C. Berger, F. Bayer, J. Brehm, L. W. Molenkamp, T. Kiessling, F. Schindler, C. H. Lee, M. Greiter, T. Neupert, and R. Thomale, Nat. Phys. **14**, 925 (2018).
[26] F. Schindler, A. M. Cook, M. G. Vergniory, Z. Wang, S. S. Parkin, B. A. Bernevig, and T. Neupert, Sci. Adv. **4**, eaat0346 (2018).
[27] J. Langbehn, Y. Peng, L. Trifunovic, F. von Oppen, and P. W. Brouwer, Phys. Rev. Lett. **119**, 246401 (2017).
[28] Z. Song, Z. Fang, and C. Fang, Phys. Rev. Lett. **119**, 246402 (2017).
[29] M. Ezawa, Phys. Rev. Lett. **120**, 026801 (2018).
[30] B. Y. Xie, H. F. Wang, H.-X. Wang, X. Y. Zhu, J.-H. Jiang, M. H. Lu, and Y. F. Chen, Phys. Rev. B **98**, 205147 (2018).
[31] J. Noh, W. A. Benalcazar, S. Huang, M. J. Collins, K. Chen, T. L. Hughes, and M. C. Rechestman, Nat. Photonics **12**, 408 (2018).
[32] M. Geier, L. Trifunovic, M. Hoskam, and P. W. Brouwer, Phys. Rev. B **97**, 205135 (2018).
[33] X. Zhang, H. X. Wang, Z. K. Lin, Y. Tian, B. Xie, M. H. Lu, Y. F. Chen, and J. H. Jiang, arXiv:1806.10028 [Nat. Phys. (to be published)].
[34] X. Ni, M. Weiner, A. Alù, and A. B. Khanikaev, arXiv:1807.00896.
[35] H. Xue, Y. Yang, F. Gao, Y. Chong, and B. Zhang, Nat. Mater. **18**, 108 (2019).
[36] X. Zhang, Z. K. Lin, H. X. Wang, Y. Tian, M. H. Lu, Y. F. Chen, and J. H. Jiang, arXiv:1811.05514.
[37] J. D. Joannopoulos, S. G. Johnson, and J. N. Winn, and R. D. Meade, *Photonic Crystals: Molding the Flow of Light - Second Edition* (Princeton University, Princeton, NJ, 2011).
[38] T. Baba, Nat. Photonics **2**, 465 (2008).
[39] A. Slobozhanyuk, S. H. Mousavi, X. Ni, D. Smirnova, Y. S. Kivshar, and A. B. Khanikaev, Nat. Photonics **11**, 130 (2017).
[40] W. P. Su, J. R. Schrieffer, and A. J. Heeger, Phys. Rev. Lett. **42**, 1698 (1979).
[41] F. Liu and K. Wakabayashi, Phys. Rev. Lett. **118**, 076803 (2017).

[42] F. Liu, H. Y. Deng, and K. Wakabayashi, Phys. Rev. B **97**, 035442 (2018).
[43] C. Poli, M. Bellec, U. Kuhl, F. Mortessagne, and H. Schomerus, Nat. Commun. **6**, 6710 (2015).
[44] See Supplemental Material at http://link.aps.org/supplemental/10.1103/PhysRevLett.122.233903 for discussions about the topological equivalence to the tight-binding model, topological theory for corner states, symmetry constraints on boundary states, phases of the corner states, boundary condition for simulation, the influence of an air layer on the band structure, and the experimental measurement, which includes Refs. [22,30,41,45–51].
[45] W. A. Benalcazar, T. Li, and T. L. Hughes, arXiv:1809.02142.
[46] F. Liu, H. Y. Deng, and K. Wakabayashi, Phys. Rev. Lett. **122**, 086804 (2019).
[47] B. Bradlyn, L. Elcoro, J. Cano, M. G. Vergniory, Z. Wang, C. Felser, M. I. Aroyo, and B. A. Bernevig, Nature (London) **547**, 298 (2017).
[48] X. Ni, M. Weiner, A. Alù, and A. B. Khanikaev, Nat. Mater. **18**, 113 (2019).
[49] H. Xue, Y. Yang, F. Gao, Y. Chong, and B. Zhang, Nat. Mater. **18**, 108 (2019).
[50] W. A. Benalcazar, B. A. Bernevig, and T. L. Hughes, Phys. Rev. B **96**, 245115 (2017).
[51] D. R. Smith, D. C. Vier, Th. Koschny, and C. M. Soukoulis, Phys. Rev. E **71**, 036617 (2005).
[52] W. Withayachumnankul, R. Yamada, C. Fumeaux, M. Fujita, and T. Nagatsuma, Opt. Express **25**, 14706 (2017).
[53] M. Weiner, X. Ni, M. Li, A. Alù, and A. B. Khanikaev, arXiv:1903.00428.
[54] M. Lin and T. L. Hughes, Phys. Rev. B **98**, 241103 (2018).
[55] M. Ezawa, Phys. Rev. Lett. **121**, 116801 (2018).
[56] M. Campbell, D. N. Sharp, M. T. Harrison, R. G. Denning, and A. J. Turberfield, Nature (London) **404**, 53 (2000).
[57] G. Harari, M. A. Bandres, Y. Lumer, M. C. Rechtsman, Y. D. Chong, M. Khajavikhan, D. N. Christodoulides, and M. Segev, Science **359**, eaar4003 (2018).
[58] M. A. Bandres, S. Wittek, G. Harari, M. Parto, J. Ren, M. Segev, D. N. Christodoulides, and M. Khajavikhan, Science **359**, eaar4005 (2018).
[59] F. F. Li, H. X. Wang, Z. Xiong, Q. Lou, P. Chen, R. X. Wu, Y. Poo, J. H. Jiang, and S. John, Nat. Commun. **9**, 2462 (2018).
[60] A. Blanco-Redondo, B. Bell, D. Oren, B. J. Eggleton, and M. Segev, Science **362**, 568 (2018).
[61] Y. Wang, X. L. Pang, Y. H. Lu, J. Gao, Z. Q. Jiao, H. Tang, and X. M. Jin, arXiv:1810.01435.
[62] J. L. Tambasco, G. Corrielli, R. J. Chapman, A. Crespi, O. Zilberberg, R. Osellame, and A. Peruzzo, Sci. Adv. **4**, eaat3187 (2018).
[63] X.-D. Chen, W.-M. Deng, F.-L. Shi, F.-L. Zhao, M. Chen, and J.-W. Dong, preceding Letter, Phys. Rev. Lett. **122**, 233902 (2019).
[64] Y. Ota, F. Liu, R. Katsumi, K. Watanabe, K. Wakabayashi, Y. Arakawa, and S. Iwamoto, arXiv:1812.10171.
[65] A. E. Hassan, F. K. Kunst, A. Moritz, G. Andler, E. J. Bergholtz, and M. Bourennane, arXiv:1812.08185.
[66] S. Mittal, V. V. Orre, G. Zhu, M. A. Gorlach, A. Poddubny, and M. Hafezi, arXiv:1812.09304.